PASJ: Publ. Astron. Soc. Japan **48**, L87–L92 and Plate 22–23 (1996)

Discovery of Hard X-Rays from a Cluster of Protostars

Katsuji KOYAMA, Kenji HAMAGUCHI, and Shiro UENO
Department of Physics, Faculty of Science, Kyoto University, Sakyo-ku, Kyoto 606-01

Naoto KOBAYASHI
National Astronomical Observatory, 2-21-1 Osawa, Mitaka, Tokyo 181
and
Eric D. FEIGELSON
Department of Astronomy and Astrophysics, Pennsylvania State University, University Park , PA 16802, U.S.A.

(Received 1996 May 23; accepted 1996 July 11)

Abstract

We report on the detection of hard X-rays from protostar candidates (Class I sources) in the R Coronae Australis (R CrA) molecular cloud. The hard X-rays are found even in the quiescent states with extremely high temperature of about 6 keV. One of the sources, probably the embedded far-infrared source R1, exhibited a powerful X-ray flare. These phenomena are similar to, but with a significantly higher temperature than, those seen in T Tauri stars. The flare spectrum is unusual, showing a broadened or double emission-line structure between 6.2 and 6.8 keV. Since X-rays are unexpected from current protostellar theory, these ASCA observations should have a significant impact on our understanding of star formation and the earliest phases of stellar evolution.

Key words: Interstellar: clouds — Stars: flares— Stars: pre–main-sequence — X-rays: sources

1. Introduction

Low-mass young stellar objects (YSOs) display a range of mm-radio to infrared excesses in their spectral energy distributions as they evolve from molecular-cloud cores through the protostellar and T Tauri stellar (henceforth TTS) phases to the main sequence. Protostars are generally associated with Class 0 and I sources, peaking respectively in the mm and mid- to far-IR domains; TTSs are associated with Class II–III infrared sources (Shu et al. 1987; Andre, Montmerle 1994). One of the surprises of X-ray imaging astronomy was the finding that TTSs emit soft X-rays at levels 10^2–10^5 brighter than that of low-mass main-sequence stars (Feigelson, DeCampli 1981; Montmerle et al. 1983). The X-ray characteristics of these T Tauri stars — moderate plasma temperatures, strong variability with occasional rapid flares — are largely consistent with an enhanced solar-type activity of a magnetic field produced by the dynamo mechanism. No current theory of star-formation predicts X-rays from protostars, the stellar evolution stages preceding the T Tauri phase, since the star-formation process is not thought to include high-energy processes. Protostars are often embedded deeply within star-forming clouds, shrouded by dense circumstellar gas and dust, and, hence, generally invisible in the optical, near-infrared, and soft X-ray bands. X-ray detection from several Class I sources has been tentatively reported from deep ROSAT and ASCA observations of the ρ Ophiuchi cloud core, although alternative Class II–III TTS identifications are possibly due to the crowded field (Casanova et al. 1995; Kamata et al. 1996). Very few photons from embedded protostars can be detected by ROSAT, since its sensitivity drops rapidly at energies above ~ 2.5 keV. ASCA images high-energy X-rays up to 10 keV and can peer deeply into star-forming clouds. However, its spatial resolution is limited for the ρ Ophiuchi core observations. Neither ROSAT nor ASCA images have revealed Xrays from three embedded protostellar sources in the Taurus L1551 cloud (Carkner et al. 1996).

The R CrA molecular cloud, at a distance of 130 pc (Marraco, Rydgren 1981), is one of the nearest dark interstellar clouds exhibiting active star formation. In addition to a loose association of TTSs, a dense grouping, called the Coronet cluster, is found near to the center of the cloud. It contains mainly Herbig Ae/Be stars, embedded Class I and a few Class II and III sources (Taylor, Storey 1984; Graham 1993). This paper reports on the first detection of hard X-rays from Class I sources or protostar candidates from the Coronet cluster.

Table 1. ASCA sources in the R CrA cloud core.

ASCA No (1)	X-ray position (α_{1950} , δ_{1950}) (2)	Count (3)	Lx (4)	Hardness ratio (5)	Optical/IR/Radio identification (6)	IR Class (7)	Optical/IR position (α_{1950} , δ_{1950}) (8)
1.....	18 58 11.8 −37 05 14	700	2.8	−0.6	CrA 1 = CD −37°13022	III	18 58 12.0 −37 05 00
2.....	18 58 16.5 −36 57 42	210	1.3	−0.7	HD 176386 = TS 2.1 = VSS 9 = GP(p)	III?	18 58 16.6 −36 57 44
3.....	18 58 18.7 −36 56 51	320	3.1	−0.6	TY CrA = TS 1.1 = VSS 5	III	18 58 18.6 −36 56 50
4.....	18 58 19.4 −37 02 47	150	1.6	0.4	IRS 2 = TS 13.1	I	18 58 19.0 −37 02 50
5.....	18 58 24.7 −37 01 36	120	2.6	0.7	IRS 5 = TS 2.4	I	18 58 25.5 −37 01 39
6.....	18 58 28.3 −37 02 19	90	3.1	0.8	IRS 1 = TS 2.6 = HH 100IR = VSS 15	I	18 58 28.2 −37 02 29
7.....	18 58 28.6 −37 00 54	70	1.8	0.8	IRS 6 = TS 2.3	II	18 58 28.0 −37 00 56
					IRS 9 = R2	I	18 58 30.7 −37 01 24
8.....	18 58 31.9 −37 01 29	190	11.7	0.9	R CrA = TS 2.10 = VSS 1	I?	18 58 31.1 −37 01 24
					IRS 7 = R1	I	18 58 32.7 −37 01 39

Column notes: (1) ASCA source number. (2) Positions from the two SIS detectors with ±20″ uncertainty in each coordinate. The position given here for source 8 is from the quiescent state. (3) Counts summed from the 39.8 ks SIS 0 exposure and the 40.0 ks SIS 1 exposure, after background subtraction and rounded to the nearest 10 counts. (4) Intrinsic X-ray luminosity in the 0.5–10 keV band from SIS 1 corrected for extinction, in units of 10^{30} erg s^{-1}. A distance of 130 pc and thermal bremsstrahlung spectra are assumed with temperatures 2×10^7 K for sources 1–3 and 7×10^7 K for sources 4–8. (5) Hardness ratio, [Ct(2–10 keV) − Ct(0.5–2 keV)]/[Ct(2–10 keV) + Ct(0.5–10 keV)], with typical error of 0.1. (6)–(7) Source names and infrared classes obtained from Taylor and Storey (1984), Walter and Kuhi (1981), Wilking et al. (1992), Walter (1986), and Wilking et al. (1986). (8) Positions from Walter (1986) for source 1 and Wilking et al. (1986) for sources 2–8.

2. Observations

The ASCA satellite pointed at the center of the Coronet cluster on 1994 April 4, and 10′ east from the center on 1994 April 8. ASCA is equipped with four thin-foil X-ray telescopes (XRT) spanning an energy range from 0.5 keV to 10 keV, and providing a cusp-shape beam at the focal plane with a resolution of 2′ full-width at half-maximum (Tanaka et al. 1994). Two X-ray CCD cameras (SIS 0 and SIS 1) and two Gas Imaging detectors (GIS 2 and GIS 3) are located on each of the focal planes. The SIS data were obtained in the 4CCD faint mode, while the GIS data were obtained in the normal PH mode. Both the SIS and GIS data were screened according to the normal selection criteria so as to exclude any data affected by the South Atlantic Anomaly, Earth occultation, and high-background regions of low-geomagnetic rigidities. We removed hot and flickering pixels from the SIS data and applied a pulse-shape discrimination technique to reject particle events in the GIS data. For an imaging analysis we mainly used the SIS data, because the spatial resolution of SIS exceeds that of GIS. For a spectral analysis, on the other hand, we preferentially used the GIS detectors, which have a higher sensitivity than the SIS at high energy above about 2 keV.

3. Results and Analysis

3.1. *Quiescent Hard X-Rays from Class I Sources*

Figure 1 shows an image taken on April 4 with the two SIS (the data of SIS 0 and SIS 1 are combined) in the 0.5–2 keV (soft band) and 4–10 keV (hard band) regions, together with a contour map of the molecular gas in those regions. The soft X-ray band image [figure 1a (Plate 22)] is similar to the Einstein Observatory IPC image (Walter, Kuhi 1981). The hard X-ray band image [figure 1b (Plate 23)] is completely different from that of the soft X-ray band. The soft band sources have almost disappeared, while a bright complex structure of about 4′ in extent appears near to the densest molecular gas. It consists of 5 local peaks. The nominal pointing error of ASCA is about 1′. By translating the ASCA image to align with the soft X-ray sources with catalogued stars, the positional uncertainty was reduced to be less than 20″. The refined hard X-ray peak positions are listed in table 1 (sources 4–8) together with those of the most probable counterparts. All five peaks coincide with the positions of Class I sources within an error of 20″. We thus conclude that the X-ray complex can be entirely attributed to these Class I sources. For a comparison, we list the soft X-ray sources (sources 1–3) in table 1, which are generally classified as Class II–III TTSs (Wilking et al. 1992).

Table 2. Spectral parameters of the Coronet cluster and CrA 1

		Coronet cluster in quiescence	Coronet cluster during flare	CrA 1
Date of observation		1994 April 4	1994 April 8	1994 April 4, 8
Thermal bremsstrahlung	kT [keV]	7.2 (4.8–12.2)	6.1 (4.0–10.8)	2.6 (2.4–2.8)
Absorption	$N_{\rm H}$ [10^{22} cm^{-2}]	4.2 (3.5–5.1)	4.3 (3.5–5.2)	0 (< 0.013)
Line 1	Energy [keV]	6.45 (6.37–6.53)	6.17 (6.07–6.27)	...
	Line flux*	2.4 (1.6–3.0)	2.8 (1.7–3.9)	...
	Equivalent width [keV]	0.8 (0.5–1.1)	0.7 (0.4–1.1)	...
Line 2	Energy [keV]	...	6.81 (6.72–6.90)	...
	Line flux*	...	3.2 (2.2–4.6)	...
	Equivalent width [keV]	...	1.1 (0.6–1.6)	...
χ^2/d.o.f.		30.7/32	30.5/25	187/99

Notes. The errors listed in parentheses are quoted for 90% confidence level.
* Line flux refers to the observed one in units of 10^{-5} photon s^{-1}cm^{-2}.

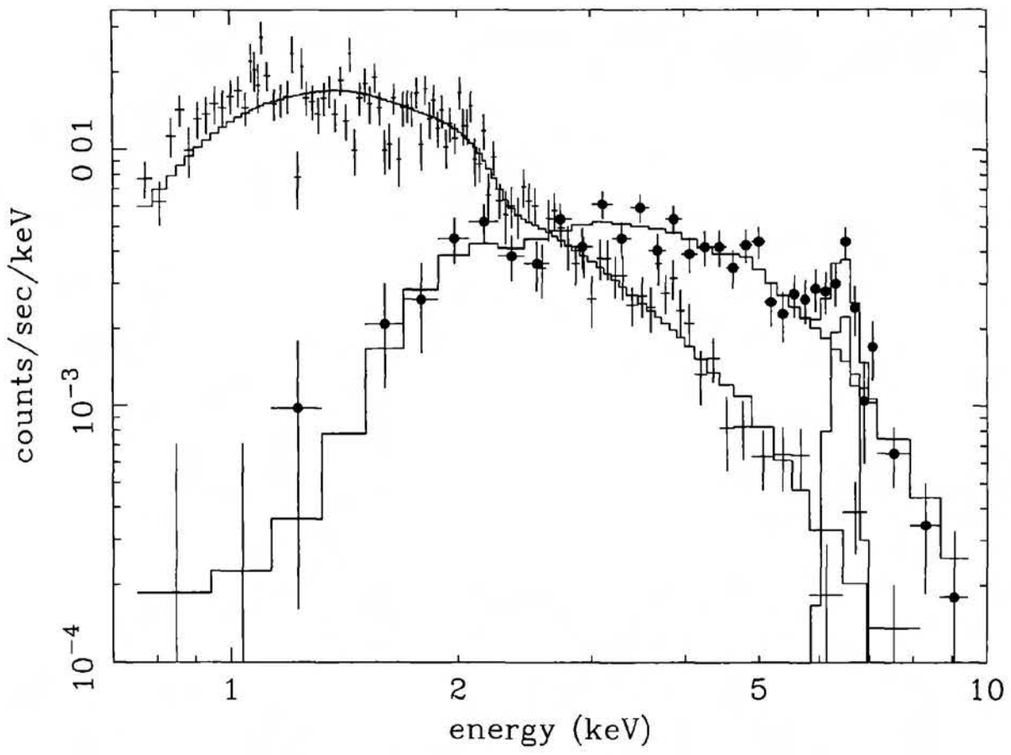

Fig. 2. Spectrum (GIS 2+3) of the Coronet cluster during the quiescent state (data are given by crosses). The histogram is the best-fit bremsstrahlung model with a Gaussian iron line and low-energy absorption, convolved with the detector response. For a comparison, the GIS spectrum of TTS CrA 1 (filled circles) is also given with the best-fit curve.

We have obtained hardness ratios using the SIS fluxes of the soft (0.5–2 keV) and hard (2–10 keV) bands, defined as follows: [Ct(2–10 keV) − Ct(0.5–2 keV)]/[Ct(2–10 keV) + Ct(0.5–2 keV)]. Depending on the spectral hardness, this value spans from −1 (when the hard flux is 0) to 1 (when the soft flux is 0). The hardness ratios of the Class I sources are all positive, while those of Class II and III are negative; the hardness ratios of the Class I sources are remarkably higher than those of Class II and IIIs sources, indicating very high temperatures as well as strong absorption for the Class I sources. To demonstrate the spectral difference between the Class I and Class II or III sources, we obtained the GIS spectra of the Coronet cluster and a Class III source CrA 1 (Walter, Kuhi 1981). The background-subtracted spectra are given in figure 2, where the background was taken from nearby source-free regions. We fit the data with a thermal bremsstrahlung model, adding lines at 6–7 keV for the Coronet cluster. The best-fit parameters are given in table 2, while the best-fit model curve is shown in figure 2. We can see a clear contrast between the Class I cluster and the Class III source: the former has an extremely high temperature ($kT \sim 7$ keV) and absorption ($N_{\rm H} \sim 4 \times 10^{22}$), while the latter has a more typical temperature ($kT \sim 2.6$ keV) and absorption ($N_{\rm H} < 10^{20}$). Using the parameter given in table 2, we list the estimated X-ray luminosity (absorption removed) of each X-ray source in table 1. We notice that, in the

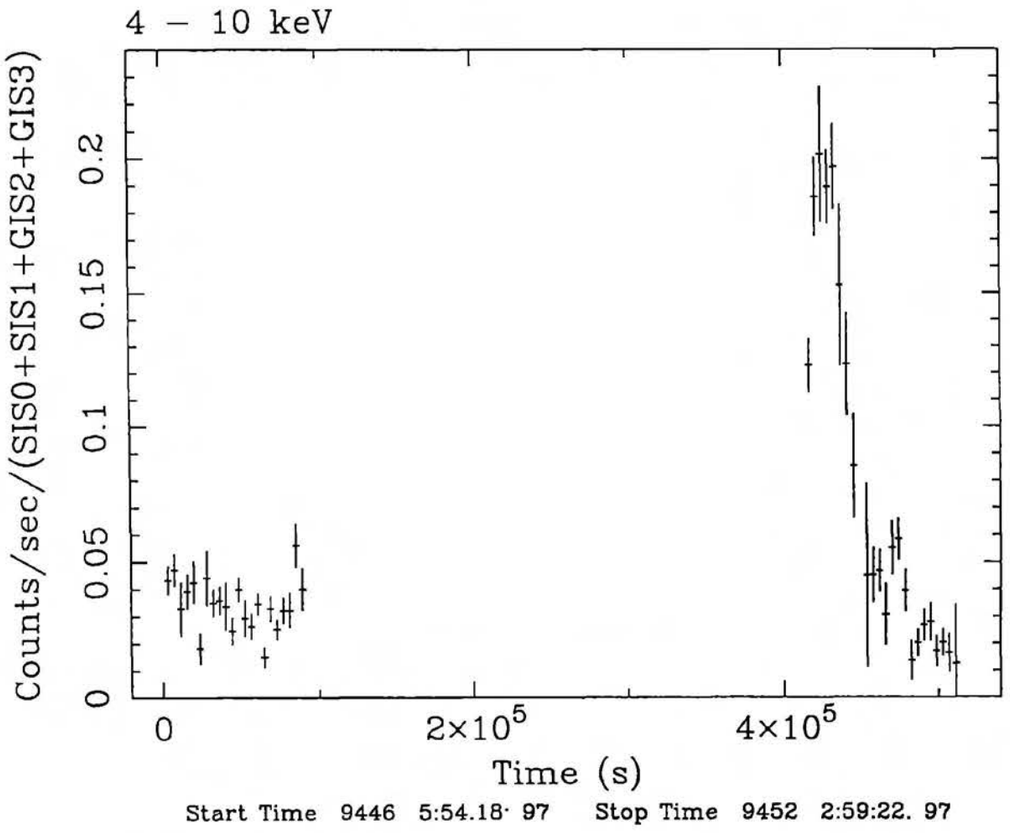

Fig. 3. X-ray light curves in the 4–10 keV band of source 8 obtained with the sum of SIS and GIS data. The photon numbers collected in every 4096 s. bins are plotted with 1-sigma error bars.

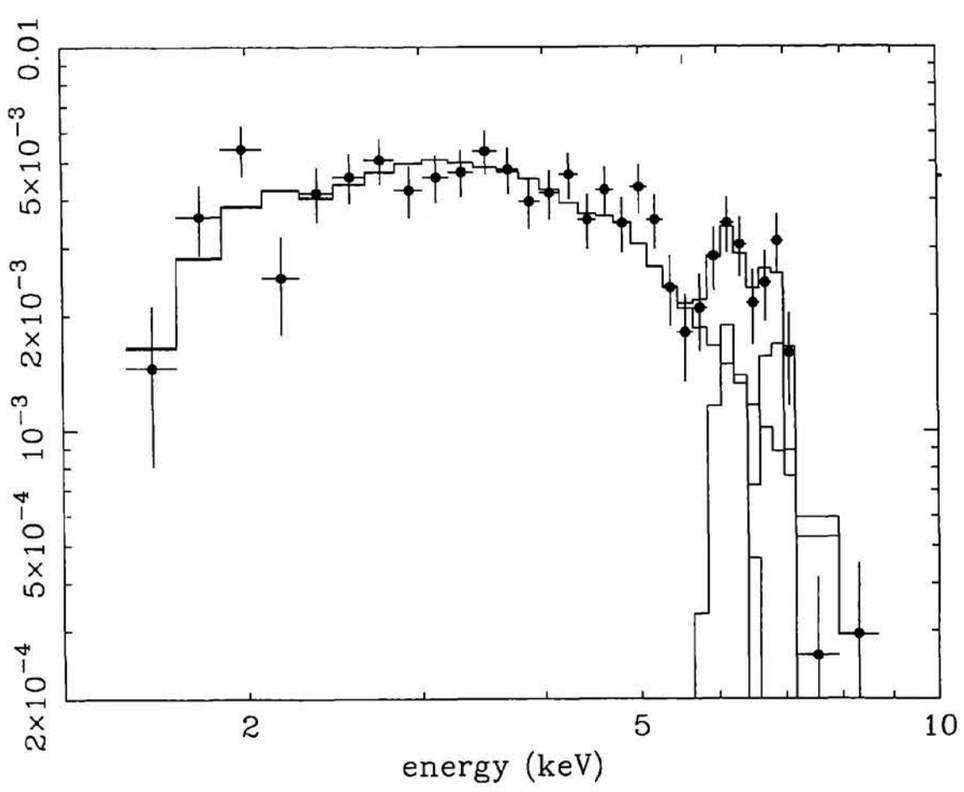

Fig. 4. Spectrum (GIS 2+3) of the Coronet cluster during the flare state. The histogram is the best-fit bremsstrahlung model with two Gaussian lines and low-energy absorption, convolved with the detector response.

Coronet cluster, virtually all Class I sources emit X-rays at levels exceeding $\sim 10^{30}$ erg s^{-1}.

The brightest location in the hard X-ray image, source 8, coincides with the densest gas in the cloud core and a compact group of YSOs, which are not resolved by the ASCA mirrors. The region includes two embedded Class Is (R1 and R2) and the optically bright Herbig Ae/Be star R CrA. At present, no Class II or III stars are known from this region. Although R CrA has a Class I spectrum, its bright visible emission requires that the stellar surface be only weakly absorbed ($A_V \sim 2.4$) (Hamann, Persson 1992a). Since the column density inferred from the X-ray spectrum of source 8 corresponds to the visible extinction $A_V \sim 10$–20 mag, we infer that it must arise from deeply embedded stars, and not R CrA. R1 is closer to the hard X-ray peak than R2, and is thus the most likely counterpart of the hard X-ray source. This identification is further strengthened by an X-ray flare found in the second ASCA observation.

3.2. X-Ray Flare from a Class I Source

During the second observation made on April 8, pointing 10′ offset from the center of the Coronet cluster, we found that the X-ray flux of source 8 increased at least by a factor of 3–4, and returned to a quiescent level, as shown in the light curve (figure 3), where the X-ray fluxes are the sum of the 4 detectors in the 4–10 keV band. This shows a typical flare shape with fast rise and slow exponential decay; the best-fit e-folding time is $(1.7 \pm 0.5) \times 10^4$ s (the errors here and below are at the 90% confidence unless otherwise mentioned). Due to heavy absorption, the flux below 2 keV is virtually zero. We note that although similar hard flares were detected in the Ophiuchus and Orion clouds with the Tenma and Ginga satellites, their lack of imaging optics prevented an identification with any individual stars (Koyama 1987; Koyama et al. 1992). An SIS image constructed from data during the hard X-ray flare shows that the position of the flare source is at $18^h\ 58^m\ 33\overset{s}{.}3$, $-37°\ 01'30''$ (1950), with a positional error of $20''$. R1 is the only catalogued source within this error circle.

The spectrum of the source 8 flare can be analyzed in some detail using the GIS data. The background spectrum is taken from the same region as that of the quiescent states. The resulting spectrum is shown in figure 4. The flare spectrum shows a surprising feature: a line complex at 6–7 keV. It has a total width of 1.3 keV FWHM, significantly greater than the instrumental resolutions of 0.6 keV FWHM (GIS). The line complex can not be an artifact of background subtraction, since the background flux is only 5% of the source flux and no structure is seen in the background spectrum at these energies. The broad line structure is independently, found in the X-ray spectra of the GIS 2 and GIS 3 detectors. The line complex therefore appears to be intrinsic to the flare. The SIS spectrum also exhibits a line structure consistent with the GIS spectrum, but does not give significant constraints due to the limited statistics. Using standard least-squares modeling methods (XSPEC software), we find that the spectrum is well-represented by the plasma described above plus two unresolved lines at

6.2 and 6.8 keV. The value of chi-squared is reduced from 71 without lines to 30 with lines, for 26 degrees of freedom; hence the presence of two lines is highly significant. The best-fit models are shown in figure 4 with the model parameters listed in table 2. The temperature ($kT \sim 6$ keV) and interstellar absorption ($N_{\rm H} \sim 4 \times 10^{22}$) during the flare are the same as those found in the quiescent state within the statistical errors. The best-fit double line energies are 6.17 ± 0.10 keV and 6.81 ± 0.09 keV, where the calibration uncertainty of the GIS instrument is estimated to be about 0.05 keV. We note that it is unclear whether or not the quiescent spectra have also broadened, or exhibit a double-line structure, due to the limited statistics.

4. Discussion

Our principal discovery is that virtually all Class I sources in the R CrA cloud core emit X-rays at levels exceeding $\sim 10^{30}$ erg s^{-1}. This ASCA observation thus shows that X-ray emission from pre–main-sequence stars is present at an earlier phase of stellar evolution than that found from previous Einstein or ROSAT studies. Surprisingly, the plasma temperature of the Class I sources are extremely high, even in the quiescent states. New astrophysical models may be needed to explain the high-temperature plasma without flaring activity. Like TTSs, one of the Class I sources R1 exhibits an X-ray flare. The X-ray flare indicates that greatly enhanced magnetic activity, already well-established in older TTSs, is present in the earlier protostellar phase. It is not evident, however, whether the protostellar magnetic fields are generated internally through a dynamo or whether they are 'fossil fields' inherited from the parent molecular cloud (Feigelson 1994). The possibility of flaring magnetic arcades rooted in a differentially rotating and turbulent circumstellar disk, or linking the star and the disk, should not be ignored (Levy, Araki 1989; Shu et al. 1994). In any case, it is difficult to see how the low-ionization and low-velocity molecular gas flows associated with low-mass star formation could generate localized and short-lived regions of $\sim 7 \times 10^7$ K plasma without an efficient process for amplifying and twisting the magnetic field lines.

Although the origin of the hard X-rays from protostars is very unclear, it is likely to have a significant impact on our understanding of the star-formation process. X-rays from the high-temperature plasma would ionize the surrounding molecular gas. This should affect the coupling of infalling gas and bipolar ejecta to ambient magnetic fields in the immediate vicinity of the X-ray emitting protostar. Protostellar X-rays may also inhibit star formation in wider environs of the molecular cloud core (Casanova et al. 1995; Silk, Norman 1983).

Another surprising fact is the presence of the double-line structures at 6.2 and 6.8 keV during the flare of R1. The 6.8 keV line can be attributed to a K-shell complex of Fe XXV and Fe XXVI in the high temperature plasma. However, the origin of the 6.2 keV emission is quite puzzling. One possibility is that these lines are red-shifted and blue-shifted K-shell iron lines in a bipolar jet. Evidence for such a jet emerges from the radio continuum morphology of the region, shown in the inset of figure 1b (Plate 23). The radio and X-ray properties (double radio morphology, hard X-ray spectrum with strong iron line) are similar to the remarkable X-ray/radio jet source SS 433 (Kotani et al. 1994). However, it is difficult to conceive how a protostar, with a gravitational potential well far weaker than that of the neutron star in SS 433, could eject material at speeds of ~ 0.1 c. Thermalization of the ~ 0.001 c inflows and outflows present around the stars R CrA and HD 176386 (Hamann, Persson 1992b; Grady et al. 1993), for example, is incapable of producing either the observed hard X-rays or the broadened iron line.

Note added in proof

After editing this proof, new results of near-infrared observations by B. Wilking (private communication) has revealed that the position of the protostar candidate IRS 7 (R1) lies within 1″ of the western radio source, IRS 7A. This new position for IRS 7 may rule out the bipolar wind interpretation for the radio source.

References

Andre Ph., Montmerle T. 1994, ApJ 420, 837
Brown A. 1987, ApJ 322, L31
Carkner L., Feigelson E.D., Koyama K., Montmerle T., Reid I.N. 1996, ApJ 464, 286
Casanova S., Montmerle T., Feigelson E.D., Andre Ph. 1995, ApJ 439, 752
Feigelson E.D. 1994, in New Horizon of X-Ray Astronomy, ed F. Makino, T. Ohashi (Universal Academy Press, Tokyo) p21
Feigelson E.D., DeCampli W.M. 1981, ApJ 243, L89
Grady C.A., Perez M.R., The P.S. 1993, A&A 274, 847
Graham J.A. 1993, PASP 105, 561
Hamann F., Persson S.E. 1992a, ApJ 394, 628
Hamann F., Persson S.E. 1992b, ApJS 82, 285
Kamata Y., Koyama K., Maeda Y., Ozaki M., Ueno S., Tawara Y., Yamauchi S. 1996, MNRAS submitted
Kotani T., Kawai N., Aoki T., Doty J., Matsuoka M., Mitsuda K., Nagase F., Ricker G., White N. 1994, PASJ 46, L147
Koyama K. 1987, PASJ 39, 245
Koyama K., Asaoka I., Kuriyama T., Tawara Y. 1992, PASJ 44, L255
Levy E.H., Araki S. 1989, Icarus 81, 74
Loren R.B., Sandqvist Aa., Wootten A. 1983, ApJ 270, 620
Marraco H.G., Rydgren A.E. 1981, AJ 86, 62
Montmerle T., Koch-Miramond K., Falgarone E., Grindlay J.E. 1983, ApJ 269, 182
Shu F., Adams F., Lizano S. 1987, ARA&A 25, 23

Shu F., Najita J., Ostriker E., Wilkin F., Ruden S., Lizano S. 1994, ApJ 429, 781
Silk J., Norman C. 1983, ApJ 272, L49
Tanaka Y., Inoue H., Holt S.S. 1994, PASJ 46, L37
Taylor K.N.R., Storey J.W.V. 1984, MNRAS 209, 5p
Walter F.M. 1986, ApJ 306, 573
Walter F.M., Kuhi L.V. 1981, ApJ 250, 254
Wilking B.A., Green T.P., Lada C.J., Meyer M.R., Young E.T. 1992, ApJ 397, 520
Wilking B.A., Taylor K.N.R., Storey J.W.V. 1986, AJ 92, 103

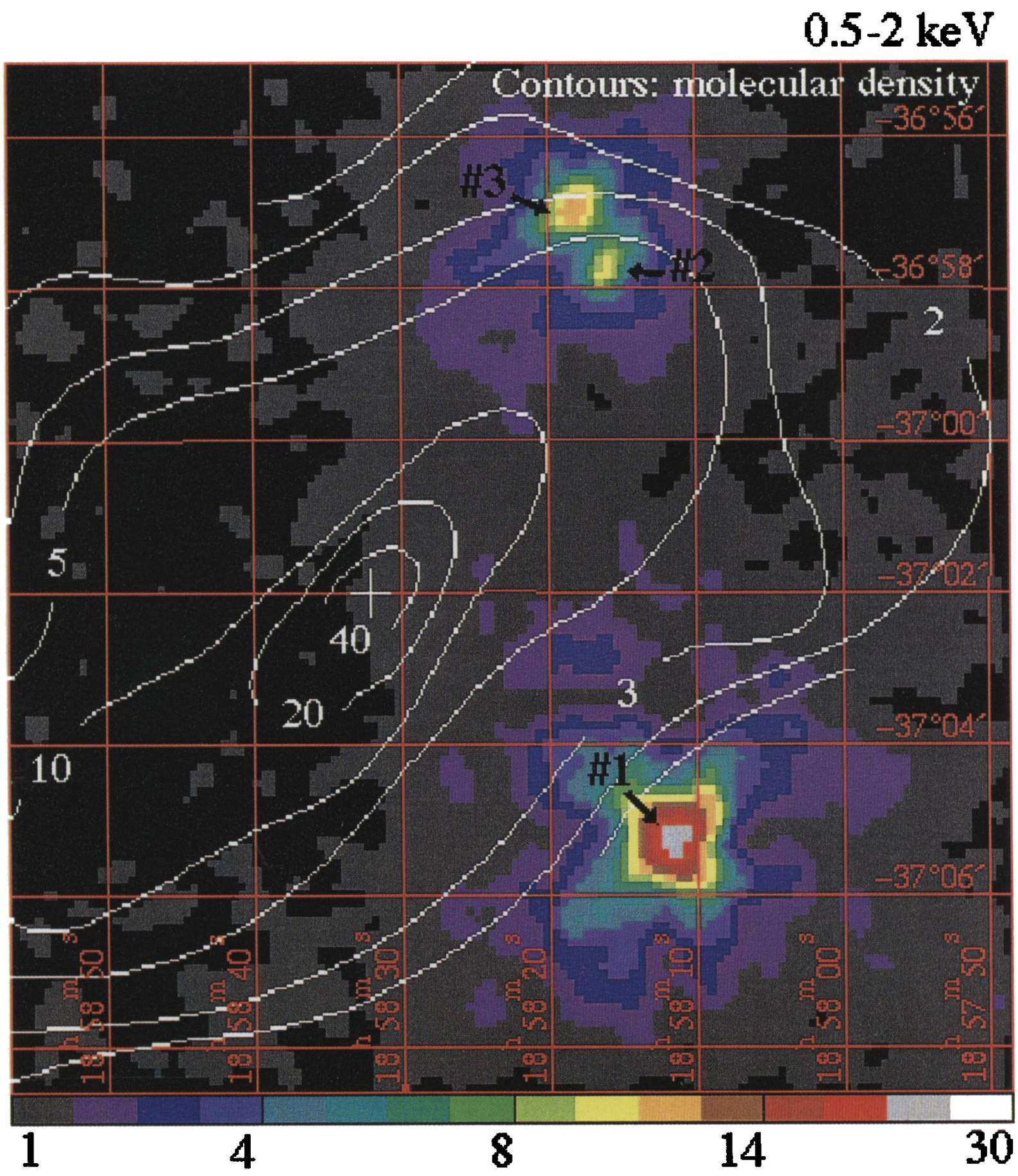

Fig. 1a. False-color images of the ASCA X-rays (SIS 0 + 1) from the Coronet cluster in the 0.5–2 keV band. The relative flux at a given color is shown in the bottom bar. The overlaid contours (Loren et al. 1983) represent the H2 volume densities in units of 10^4 cm^{-3}. The southwest source is a TTS CrA 1 discovered with the Einstein satellite (Walter, Kuhi 1981), while the two closely spaced sources to the northwest are HD 176386 and TY CrA.

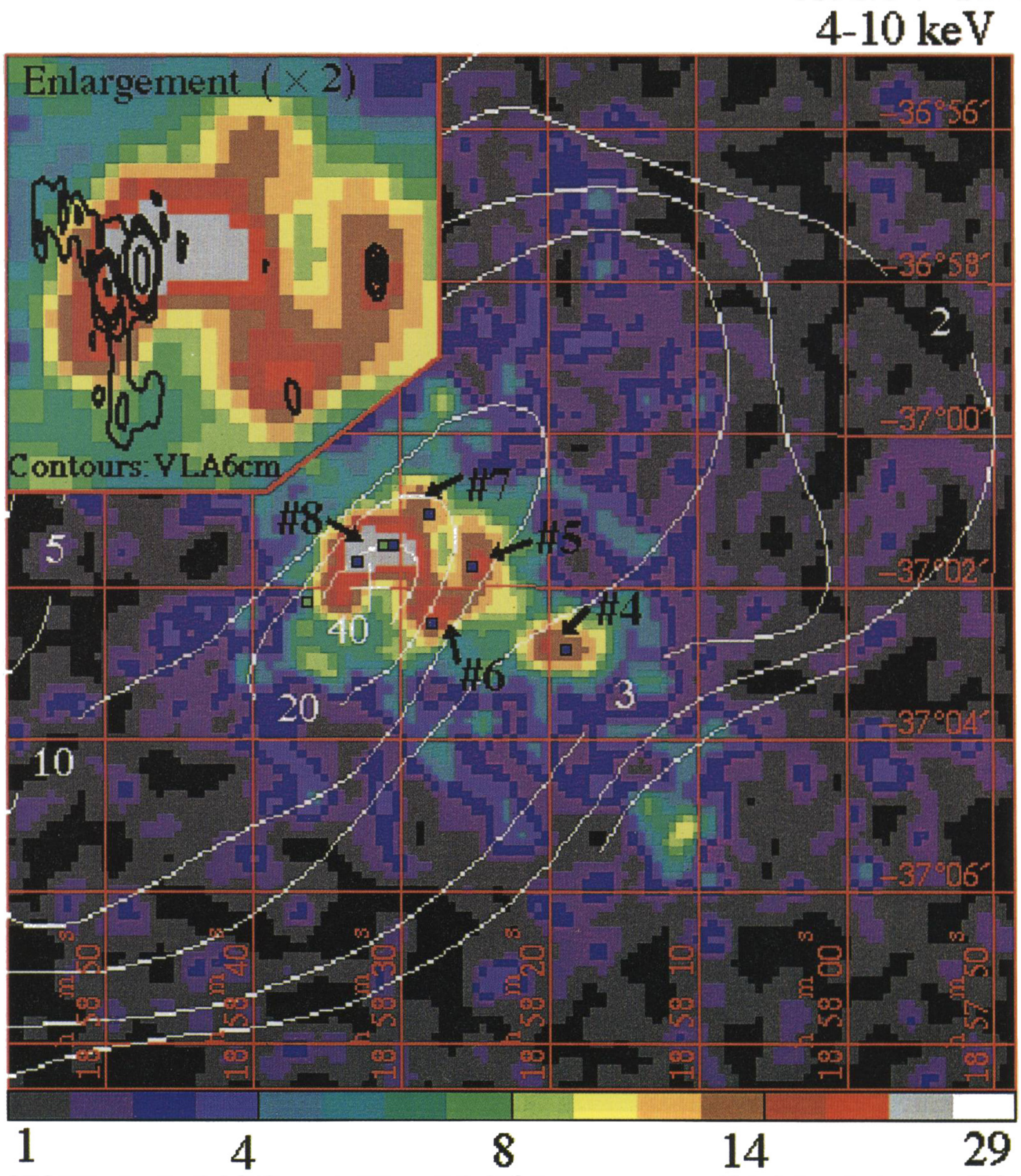

Fig. 1b. Same as figure 1a, but for the 4–10 keV bands. The green squares are embedded Class I infrared sources, while the blue squares are Class II and III sources. The inset shows contours from the VLA radio continuum map (Brown 1987) superposed on the cluster of hard X-ray sources.